I&EC research
Industrial & Engineering Chemistry Research

pubs.acs.org/IECR
Article

Sustainable Development Goals-Based Prospective Process Design Using Hybrid Modeling

Published as part of Industrial & Engineering Chemistry Research special issue "AI/ML in Chemical Engineering".

Sachin Jog, Daniel Vázquez, Lucas F. Santos, Juan D. Medrano-García, and Gonzalo Guillén-Gosálbez*

Cite This: *Ind. Eng. Chem. Res.* 2025, 64, 2816−2830

Read Online

ACCESS | Metrics & More | Article Recommendations | Supporting Information

ABSTRACT: Replacing fossil technologies with renewable carbon-based technologies is of vital importance for the development of sustainable chemical processes in the future. However, impacts beyond climate change should be carefully evaluated to ensure that this transition to defossilized chemicals is truly sustainable. Here, we develop a framework for sustainable process design that explicitly accounts for the performance attained in the Sustainable Development Goals (SDGs), which is computed using standard life cycle assessment (LCA) metrics alongside the planetary boundaries (PBs) concept. We apply this approach to design a CO_2 hydrogenation to methanol process, where economic and SDGs-based performance are the objectives optimized. We show that the environmentally optimal design reduces the impact on SDG 13 (climate action) substantially relative to the business-as-usual (BAU) fossil counterpart, yet this is done at the expense of worsening other categories. A prospective LCA reveals that such collateral damage will be drastically reduced in the future due to improvements in a range of economic sectors. Overall, this work highlights the need to embrace impacts beyond climate change in process design and the advantages of using hybrid surrogates to expedite the computation of Pareto designs.

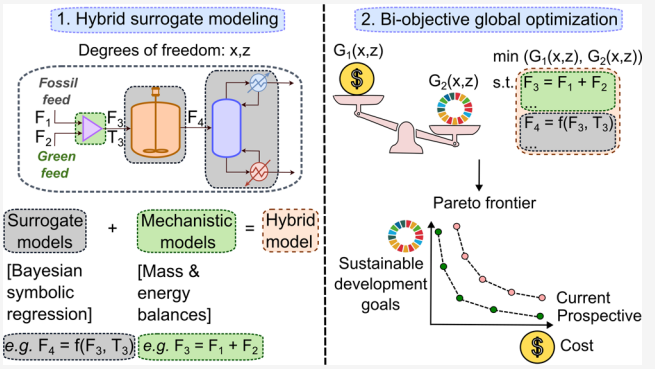

INTRODUCTION

With the adoption of the Paris Agreement[1] in 2015, it has become imperative for the chemical industry, accounting for approximately 10% of global anthropogenic CO_2 emissions,[2] to gradually transition to more sustainable production pathways. Consequently, it is crucial to consider environmental metrics when analyzing current fossil carbon-based processes and designing alternative, cleaner chemical production pathways (e.g., based on carbon capture and utilization (CCU), waste and biomass conversion, etc.).

Thus, in this context, life cycle assessment (LCA) has emerged as an important tool to quantify the environmental performance of a product or service over its full life cycle.[3] The ReCiPe,[4] IMPACT,[5] and Environmental Footprint (EF[6]) methods (among others) are examples of LCA-based approaches that were applied to chemical systems. Moreover, the field of life cycle optimization[7] (LCO), i.e., LCA coupled with process optimization, has gained wide attention in the Process Systems Engineering (PSE) community, finding applications in the multi-objective optimization of supply chains,[8−10] energy networks,[11] and process design,[12−14] among other fields. Furthermore, prospective LCAs have recently emerged to evaluate how future climate scenarios will affect the performance of chemical systems. In this regard, Boyce et al.[15] analyzed global ammonia decarbonization scenarios, concluding that while up to 70% reduction could be achieved in climate impacts, complete decarbonization of this sector is unlikely by 2050. Moreover, Nabera et al.[16] presented regionalized prospective LCAs of key platform chemicals, concluding that green routes could achieve up to 90% carbon emissions reductions.

Traditional LCA damage assessment indicators used in LCO for process design, such as ReCiPe and IMPACT, can be used to compare alternative technologies. However, they provide limited insights into whether technologies are truly sustainable in absolute terms, i.e., considering the limited carrying capacity of the Earth. To overcome this limitation, maximum allowable

Received: September 20, 2024
Revised: November 27, 2024
Accepted: January 3, 2025
Published: January 21, 2025

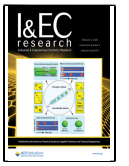

https://doi.org/10.1021/acs.iecr.4c03563
Ind. Eng. Chem. Res. 2025, 64, 2816−2830

limits on impact categories were recently defined for conducting absolute sustainability assessments. These limits establish thresholds consistent with the planet's ecological capacity that define a "safe operating space" (SOS) within which all anthropogenic activities should coexist. In this context, the planetary boundaries (PBs) framework[17,18] provides a set of thresholds on nine Earth system processes key for maintaining the Earth's resilience. Transgressing these limits could trigger detrimental events, potentially causing the Earth to transition to a more harmful and unpredictable state.[18] Absolute sustainability assessments based on the PBs framework were performed in process design,[19] energy systems,[20] supply chains,[21] as well as process optimization.[22] More recently, the concept of absolute sustainability was employed to quantify the performance attained by engineering systems on the 17 Sustainable Development Goals[23] (SDGs). Adopted by 193 member states of the United Nations (UN) in 2015, these goals serve as a guideline for policymakers to combat the critical challenges facing humanity. Notably, Sala et al.[24] recently introduced an LCA-PBs-based framework, which combines the SDGs with the EF method by linking nine PBs and five SDGs to the 16 LCA impact categories of the EF method. This framework was used to assess low-carbon technologies in the chemical industry by Ioannou et al.,[25] where the authors applied linear programming (LP) and LCA to study how to optimally produce carbon-neutral chemicals. To the best of our knowledge, however, these SDG metrics were never applied to process design.

From the process modeling viewpoint, sustainable process design has been often performed using monolithic formulations and, more recently, simulation-optimization approaches and surrogate models.[22,26] The latter can be constructed using a variety of techniques, such as artificial neural networks (ANNs), random forests, kriging, etc. In recent years, the field of symbolic regression, which can represent any closed-form mathematical equation as an expression tree,[27] has also attracted interest. Different techniques such as genetic programming[28] and disjunctive programming[29] can be used to construct these mathematical expressions from data. Alternatively, Guimerà et al.[30] introduced the Bayesian machine scientist (BMS), which uses Markov chain Monte Carlo (MCMC) sampling to generate closed-form expressions from data. The BMS was recently employed in the global optimization of process flowsheets by Forster et al.,[31] who showed that analytical surrogates are easier to optimize but the associated model-building task becomes more computationally demanding.

Further, Psichogios and Ungar[32] showed that a direct mapping between process inputs and outputs without considering process knowledge (i.e., a "black-box" model) can lead to a surrogate model that overfits and has poor generalization capabilities. This has led to works that approach process optimization using hybrid modeling, i.e., models complementing data-driven black-box models (which can be created using e.g., ANNs[33,34] and kriging[35,36]) with mechanistic equations. In a previous work,[37] we used Bayesian symbolic regression (the BMS) to create hybrid analytical surrogates for the global optimization of process flowsheets. As in the purely black-box case mentioned above,[31] we found that the CPU time savings in the surrogate optimization cannot offset the extra time required for model building. This might not be the case in multi-objective optimization, where multiple single-objective models need to be solved when deterministic methods are employed to approximate the Pareto frontier.[38]

Here, we apply SDG metrics to process design and employ analytical hybrid models to solve the resulting bi-objective problem. The main novelty of this work lies in the way we compute the second objective function, i.e., the sustainability performance of the process. Most of the previous works have focused on traditional LCA methodologies,[12−14] while others applied the PBs framework.[19,22] Instead, here we use the performance relative to the SDGs, which are highly relevant in policy-making, to evaluate the sustainability performance of process designs. We compare our results with a derivative-free multi-objective optimization algorithm, focusing on methanol production using CO_2 hydrogenation as a testbed problem. Additionally, we also discuss the environmental performance of methanol production in current and prospective scenarios to study the expected temporal changes in process performance over time. The structure of the article is as follows. We begin by describing the problem statement and methodology adopted in this work, followed by a description of the case study and its associated results. In the last section, we present the conclusions of the work.

PROBLEM STATEMENT

The goal of this work is to provide a framework for the optimal design and operation of sustainable chemical processes considering their impact on the SDGs and cost. More precisely, given a set of technical and product quality constraints, the goal is to find the process topology, sizes of units, and operating conditions that maximize the performance attained on the SDGs and the cost. We consider production cost as the economic criterion, while, for the environmental criterion, we adopt absolute sustainability assessment methods to study the impacts of the chemical production process on the SDGs. In the following sections, we describe how we solve this problem.

METHODOLOGY

We formulate the process design task as a bi-objective optimization problem with the following general form:

$$\begin{aligned} &\min(F_1(x, z), F_2(x, z)) \\ &\text{s. t. } h(x, z) = 0 \\ &\quad g(x, z) \le 0 \\ &\quad \underline{x} \le x \le \overline{x} \\ &\quad \underline{z} \le z \le \overline{z} \\ &\quad x \in R^n, z \in Z^n \end{aligned} \tag{1}$$

where $F_1(x,z)$ and $F_2(x,z)$ are the two objective functions to be minimized that depend on continuous variables x and integer variables z. Continuous variables denote the operating conditions of the process (such as temperatures, pressures, etc.), while integer variables represent design variables (such as the number of stages in a distillation column). The equality and inequality constraints are denoted by $h(x, z)$ and $g(x, z)$ respectively. The lower bounds of the continuous and integer variables are denoted by $\underline{x}$ and $\underline{z}$, respectively, while their respective upper bounds are denoted by $\overline{x}$ and $\overline{z}$.

As objective functions, we use the unitary production cost and the mean transgression level (MTL) of a set of LCA metrics. The MTL is an environmental performance indicator

https://doi.org/10.1021/acs.iecr.4c03563
Ind. Eng. Chem. Res. 2025, 64, 2816−2830

that quantifies the transgression of the SOS by the production process, as explained in further detail in the following sections. Moreover, we carry out a prospective LCA to analyze the expected changes in environmental performance in 2050, assuming a specific future climate scenario, as described later in the article.

As shown in our previous work[37] and discussed in detail later, we can model the process in Equation 1 via hybrid surrogates. The hybrid (HY) model consists of two complementary parts: a data-driven component generated using the BMS, and a mechanistic part based on mass and energy balances defined for the flowsheet. The resultant HY model is then optimized following the ε-constraint algorithm[38] to obtain a Pareto frontier of optimal designs.

Our modeling and solution approach (shown schematically using the flowchart in Figure 1) is outlined below, with a strong emphasis on how we quantify sustainability performance based on the SDGs.

Modeling the Economic and Environmental Objective Functions. As mentioned previously, the main novelty of this work concerns the method for computing the sustainability performance of the process. To this end, we capitalize on the work by Sala et al.,[24] which introduced a methodology for absolute sustainability assessment based on the SDGs. In essence, we leverage this methodology to analyze the potential impact of the chemical process on the attainment of the SDGs. We now discuss the general formulation of the two objective functions, while specific details for the studied process are described in the Case Study section.

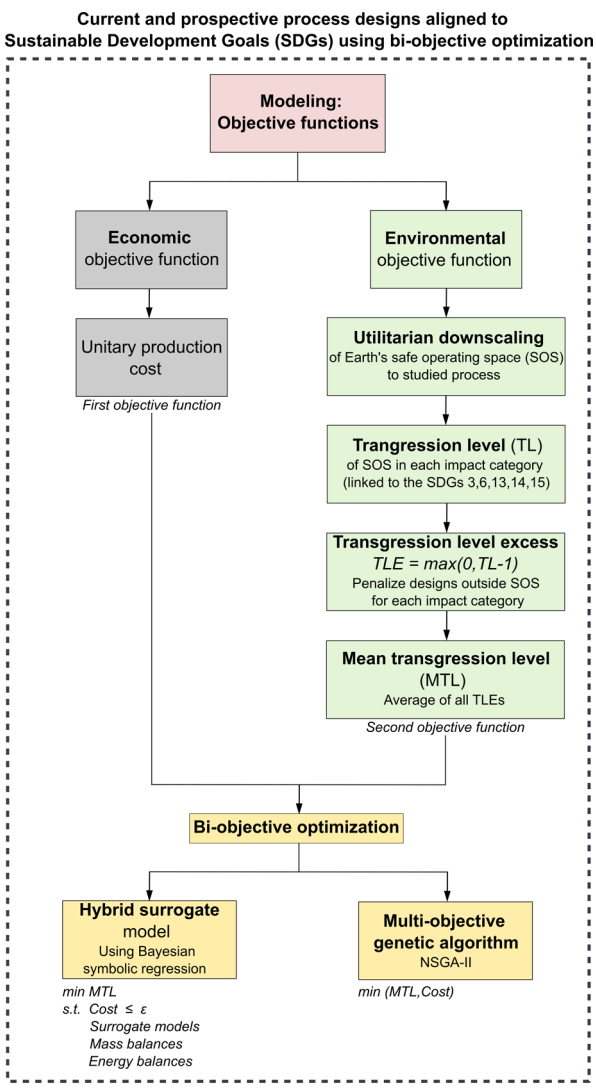

Figure 1. Methodology for current and prospective process designs aligned to Sustainable Development Goals using bi-objective optimization.

Concerning the economic objective function (F_1), we calculate the unitary production cost, accounting for the operating expenditures (OPEX).

The environmental objective function (F_2) is based on the MTL, for which we use the impact categories k defined by the EF v3.1 LCA method recommended by the European Union (EU). The functional unit is 1 kg of the final product. To calculate F_2, we first define the life cycle inventory (LCI) of feed, utilities, waste, and emissions of the process, which is obtained by combining data from the foreground system (i.e., mass and energy flows from the process simulation) with the background system (i.e., an environmental database). Thus, each LCI entry m in the set M can be defined as follows:

$$\mathrm{LCI}_m = \sum_{r\in R} \mathrm{LCA}_{m,r}^{\mathrm{RM}}\cdot \mathrm{RM}_r + \sum_{t\in T} \mathrm{LCA}_{m,t}^{\mathrm{UTI}}\cdot \mathrm{UTI}_t + \mathrm{LCA}_m^{\mathrm{WASTE}} + \mathrm{LCA}_m^{\mathrm{DIR}} \quad \forall\, m \in M \tag{2}$$

Here, $\mathrm{LCA}_{m,r}^{\mathrm{RM}}$, $\mathrm{LCA}_{m,t}^{\mathrm{UTI}}$, $\mathrm{LCA}_m^{\mathrm{WASTE}}$, and $\mathrm{LCA}_m^{\mathrm{DIR}}$ denote the LCI entries corresponding to a unit of raw material r (in the set of raw materials R), utility t (in the set of utilities T), waste, and direct emissions, respectively. RM_r and UTI_t are the amounts of raw materials and utilities consumed per unit of the final product, i.e., the functional unit, respectively. Next, the impact for category k (IMP_k) (in unit·kg^{-1}) is defined by combining the LCI entries with the characterization factors of each LCI entry for each category ($\mathrm{CF}_{k,m}$), as shown in Equation 3 below. Here, $k \in K$, where K is the set of impact categories. The impact categories with their associated units and SOS values are shown in Section E of the Supporting Information.

$$\mathrm{IMP}_k = \sum_{m\in M} \mathrm{LCI}_m\cdot \mathrm{CF}_{k,m} \quad \forall\, k \in K \tag{3}$$

Next, the transgression level (TL) of each impact category (TL_k) is defined as the ratio of IMP_k over the share of the safe operating space (SOS_k) given by the PBs and allocated to the studied system. In an absolute sustainability assessment, the SOS refers to the total carrying capacity of the Earth. Therefore, while carrying out this assessment for one production process, it is necessary to downscale it to our system, i.e., for the product being analyzed, as done in previous works.[22,39−41] We follow the same principle as in Vázquez and Guillén-Gosálbez,[22] applying a utilitarian downscaling based on the Gross Value Added (GVA) of the studied product and that of the world ($\mathrm{GVA}_{\mathrm{product}}$ and $\mathrm{GVA}_{\mathrm{world}}$, respectively). Thus, we allocate a share of the Earth's carrying capacity to the methanol process based on its economic contribution to the global economy. Here, we note that the GVA is assumed to be defined through the worldwide revenue from methanol production, as the GVA of methanol is not directly reported (the GVA should consider the net profit, but these company-specific data are unavailable in the public domain). Therefore, we acknowledge that the TL of methanol production is underestimated due to this assumption. The SOS is thus

https://doi.org/10.1021/acs.iecr.4c03563
Ind. Eng. Chem. Res. 2025, 64, 2816−2830

downscaled using a downscaling factor α, calculated from the ratio between the GVA of the studied product and the global GVA. Note that this is an important assumption, as the results obtained are linked to the type of downscaling principle used. Therefore, in what follows, the SOS linked to each SDG always refers to this downscaled SOS. We also note that there are other downscaling principles that can be applied,[42] the selection of which lacks scientific consensus.[22] This downscaling factor α and the TLs are defined as shown in Equations 4 and 5, respectively:

$$\alpha = \frac{\mathrm{GVA}_{\mathrm{product}}}{\mathrm{GVA}_{\mathrm{world}}} \tag{4}$$

$$\mathrm{TL}_k = \frac{\mathrm{IMP}_k}{\alpha \cdot \mathrm{SOS}_k} \quad \forall\, k \in K \tag{5}$$

A TL above 1 means that the process transgresses the downscaled SOS, making it unsustainable. Therefore, we only penalize the TLs above 1, hence defining a transgression level excess (TLE) for each LCA indicator k (TLE_k) as follows:

$$\mathrm{TLE}_k = \max(0,\ \mathrm{TL}_k - 1) \quad \forall\, k \in K \tag{6}$$

We reformulate Equation 6 using the following inequalities:

$$\begin{aligned} &\mathrm{TLE}_k \geq \mathrm{TL}_k - 1 \quad \forall\, k \in K \\ &\mathrm{TLE}_k \geq 0 \qquad\quad \forall\, k \in K \end{aligned} \tag{7}$$

The second objective function (F_2) is thus an average of the TLE of each LCA indicator, i.e., the MTL, and is defined as follows:

$$F_2 = \mathrm{MTL} = \frac{\sum_{k=1}^{n} \mathrm{TLE}_k}{|K|} \tag{8}$$

Here, we use 14 LCA impact categories defined in the EF v3.1 method, and the updated LANCA[43] v2.5 model for the land use category. The SOS for each impact category is obtained from the work by Sala et al.,[24] while the impacts related to human health are updated according to the world population (as shown in Section E of the Supporting Information). The current design of the CO_2 hydrogenation process is termed the current scenario, which is computed assuming the most recent LCA data available. For the prospective LCA (called the prospective scenario), Integrated Assessment Models (IAMs) such as IMAGE[44] (Integrated Model to Assess the Global Environment) offer a thorough understanding of the relationships between society, biosphere, and the climate systems, which can be used to study different future climate scenarios according to the IAM's economic projections. With results from IMAGE, we construct future background data using the *premise*[45] v2.1.0 framework. Moreover, the IMAGE model assumes specific shared socio-economic pathways (SSPs) and representative concentration pathways (RCPs), that define climate change mitigation scenarios. Accordingly, we consider the more ambitious RCP1.9 scenario under SSP2 (middle-of-the-road), aiming to limit the global mean surface temperature rise to 1.5 °C (SSP2-RCP19 scenario in *premise*). Further, the cost parameters have been kept the same as for the current scenario, owing to the difficulty in predicting the prices of raw materials and utilities in 2050 precisely and also due to the focus being on the environmental performance. Additionally, we do not modify the downscaling factor α for 2050 due to the uncertainty in predicting the GVA of methanol production and the world.

Hybrid Process Modeling. In this section, we describe the methodology adopted for surrogate modeling and bi-objective optimization of the process flowsheet. The single-objective hybrid modeling approach was already presented in depth elsewhere,[37] yet we provide a general description for completeness. We also extend the framework to handle multiple objectives, explaining how we compare with another modeling and optimization method.

Data Sampling and Surrogate Modeling of the Process Flowsheet. We use Latin hypercube sampling (LHS) to generate the training and test data sets to be used for the surrogate modeling. The values of these degrees of freedom are sent to the process simulator for each successive point of the data sets, storing the outputs only if the simulation converges.

In the hybrid modeling approach, we model some of the units in the flowsheet with analytical surrogates, which are inserted into a mathematical backbone, including mass and energy balances defined for the system and its components. The general formulation of these surrogates that provide specific outputs for the HY model is shown in Equation 9:

$$\begin{aligned} x_c = m_{ij}\left(x_{c' \in \mathrm{IM}_{ij}^{C}},\ d_{u \in \mathrm{IM}_{ij}^{U}},\ y_{z \in \mathrm{IM}_{ij}^{Z}}\right) \\ \forall\, i \in I,\ j \in JI_i,\ c \in \mathrm{OM}_{ij} \end{aligned} \tag{9}$$

where the values of the continuous process variables, continuous structural variables, and integer variables are denoted by x_c, d_u, and y_z, respectively. The continuous process variables c, continuous structural variables u, and integer variables z are contained in the sets C, U, and Z, respectively. Equation 9 shows the general formulation of surrogate models for variables x_c (note that this is the only variable type represented using surrogate models), where m_{ij} is the function that denotes the input-output relationship. Here, I represents the set of process units i which are replaced with surrogate process models, while J denotes the set of surrogate process models j for each process unit i. Each surrogate process model j of process unit i is defined by the subset $JI_i \subset J$. Further, $IM_{ij}^{C} \subset C$ denotes the subset of continuous process variables c that are fed to model j of process unit i. Similarly, $IM_{ij}^{U} \subset U$ and $IM_{ij}^{Z} \subset Z$ are analogous to IM_{ij}^{C} for the continuous structural and integer variables, respectively. All three subsets of input variables are defined for every process model j and its associated process unit i. $OM_{ij} \subset C$ denotes the subset of continuous process variables c that are obtained as the output of process unit i in model j.

Analysis of the Surrogate Model Accuracy. The coefficient of determination (R^2), mean squared error (MSE), and mean absolute percentage error (MAPE) are used to quantify the errors in the training and test sets of each surrogate model. These metrics are calculated as shown in Equation 10:

$$\begin{aligned} R^2 &= 1 - \frac{\sum_{i=1}^{n} (y_i - \hat{y}_i)^2}{\sum_{i=1}^{n} (y_i - \bar{y})^2} \\ \mathrm{MSE} &= \frac{1}{n} \sum_{i=1}^{n} (\hat{y}_i - y_i)^2 \\ \mathrm{MAPE} &= \frac{1}{n} \sum_{i=1}^{n} \frac{|(y_i - \hat{y}_i)|}{y_i} \end{aligned} \tag{10}$$

https://doi.org/10.1021/acs.iecr.4c03563
Ind. Eng. Chem. Res. 2025, 64, 2816−2830

Each data point is denoted by i, while the total number of data points is n. The actual output value, predicted output value, and the mean of the actual output values are denoted by y_i, $\hat{y}_i$, and $\overline{y}$, respectively. By actual output value, we mean the values obtained from the rigorous simulation.

Solution Procedure, Postoptimal Analysis, and Software Implementation. *Bi-objective Optimization of the HY Model.* The general mathematical formulation for the bi-objective optimization of the HY model entails solving iteratively the following optimization problem according to the ε-constraint method:[38]

$$\begin{aligned}
&\min\ f_1^{\mathrm{HY}}(x_c, d_u, y_z)\\
&\text{s.t.}\quad f_2^{\mathrm{HY}}(x_c, d_u, y_z) \le \varepsilon\\
&x_c = m_{ij}(x_{c'\in IM_{ij}^C}, d_{u\in IM_{ij}^U}, y_{z\in IM_{ij}^Z})\ \ \forall\ i \in I, j \in JI_i, c \in OM_{ij}\\
&h(x_c, d_u, y_z) = 0\\
&g(x_c, d_u, y_z) \le 0\\
&\underline{x_c} \le x_c \le \overline{x_c}\\
&\underline{d_u} \le d_u \le \overline{d_u}\\
&\underline{y_z} \le y_z \le \overline{y_z}\\
&x_c, d_u \in R^n, y_z \in Z^+
\end{aligned} \tag{11}$$

Here, $f_1^{\mathrm{HY}}(x_c, d_u, y_z)$ is the objective function to be optimized, while the other objective function $f_2^{\mathrm{HY}}(x_c, d_u, y_z)$ is modeled as a constraint. The parameter ε is varied to find Pareto-optimal solutions to the bi-objective optimization problem.[46] The second constraint is the data-driven part of the HY model and contains the surrogate models as defined in Equation 9. The explicit equality constraints $h(x_c, d_u, y_z)$ denote the mechanistic equations (such as mass and energy balances), i.e., the mechanistic part of the HY model, while the inequality constraints $g(x_c, d_u, y_z)$ are defined for imposing conditions on process variables (e.g., product purity). The lower and upper bounds of the three variable types are denoted by x_c, d_u, and y_z, and $\overline{x_c}$, $\overline{d_u}$, and $\overline{y_z}$, respectively.

Note that the solutions obtained from the bi-objective optimization for the extreme points could be degenerate; i.e., there could be a feasible solution with the same value of $f_2^{\mathrm{HY}}(x_c, d_u, y_z)$, but a lower value of $f_1^{\mathrm{HY}}(x_c, d_u, y_z)$, or vice versa. To ensure that the solution found is strongly Pareto optimal, i.e., no other solution exists with at least a better value of one objective and the same value for the other, we proceed as follows. We first optimize one objective, e.g., $f_1^{\mathrm{HY}}(x_c, d_u, y_z)$. We then minimize the other objective, $f_2^{\mathrm{HY}}(x_c, d_u, y_z)$, forcing $f_1^{\mathrm{HY}}(x_c, d_u, y_z)$ to be equal to the optimal value found in the first run.

Comparison with a Multi-objective Derivative-Free Optimization Algorithm. As described in the previous section, the Pareto-optimal solutions using the HY model are found by successively optimizing single-objective reformulations of the multi-objective optimization problem. However, multiple Pareto-optimal solutions can also be found simultaneously in a single optimization run using multi-objective evolutionary algorithms,[47] such as the Vector Evaluated Genetic Algorithm[48] (VEGA), Nondominated Sorting Genetic Algorithm[49] (NSGA), and the Nondominated Sorting Genetic Algorithm II[50] (NSGA-II). The NSGA algorithm is based on nondominated sorting,[51] where a ranking selection method emphasizes good points, while a niche method maintains stable subpopulations of good points. Here, we use the NSGA-II algorithm (called GA hereafter) for the bi-objective optimization problem, comparing the Pareto-optimal solutions obtained from it with those obtained from the optimization of the HY model.

Analysis of the Bi-objective Optimization Results. After the optimization of the HY model is completed, we insert the optimized values of the degrees of freedom back into the simulation to obtain the true values of both objective functions f_1^{HY} and f_2^{HY} (denoted by F_1 and F_2, respectively). We thus obtain the percentage deviations (D_1 and D_2) between the objective functions obtained from the surrogate model and rigorous simulation, which are defined as follows:

$$\begin{aligned}
D_1[\%] &= \frac{|F_1 - f_1^{\mathrm{HY}}|}{F_1} \times 100\\
D_2[\%] &= \frac{|F_2 - f_2^{\mathrm{HY}}|}{F_2} \times 100
\end{aligned} \tag{12}$$

Note that we do not need to define a percentage deviation for the GA as we directly optimize the flowsheet without constructing a surrogate model.

To compare the Pareto fronts obtained using both optimization models in quantitative terms, we use the hypervolume indicator,[47] which calculates the area dominated by the Pareto efficient solutions with respect to a user-defined reference point, as shown with the help of an example for two objective functions F_1 and F_2 in Figure 2. Here, the dominant Pareto frontier has an additional area (shaded with hatched lines) with respect to the reference point.

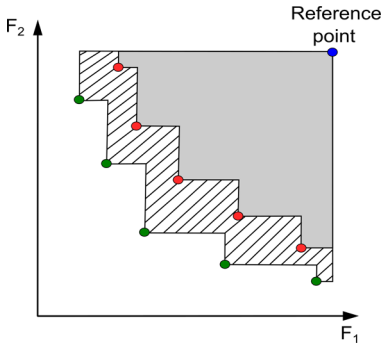

Figure 2. Computation of the hypervolume indicator for two Pareto frontiers.

To specify the reference point, we use the formula proposed by Ishibuchi et al.,[52] for which the two objective functions are first normalized. Thereafter, the reference point is defined as (r, r), where $r = 1 + \frac{1}{(m-1)}$, with m being the number of Pareto-optimal points.

Software Implementation. All calculations are done on an Intel Core i7 10700 CPU @ 2.90 GHz computer. The process flowsheet has been developed in Aspen Plus® v11, with 500 and 125 converged data points generated via LHS in pyDOE v0.3.8 for the training and test data sets, respectively. The surrogate models are then created using the training data set through the BMS (with 6,000 MCMC steps) run in Python

https://doi.org/10.1021/acs.iecr.4c03563
Ind. Eng. Chem. Res. 2025, 64, 2816−2830

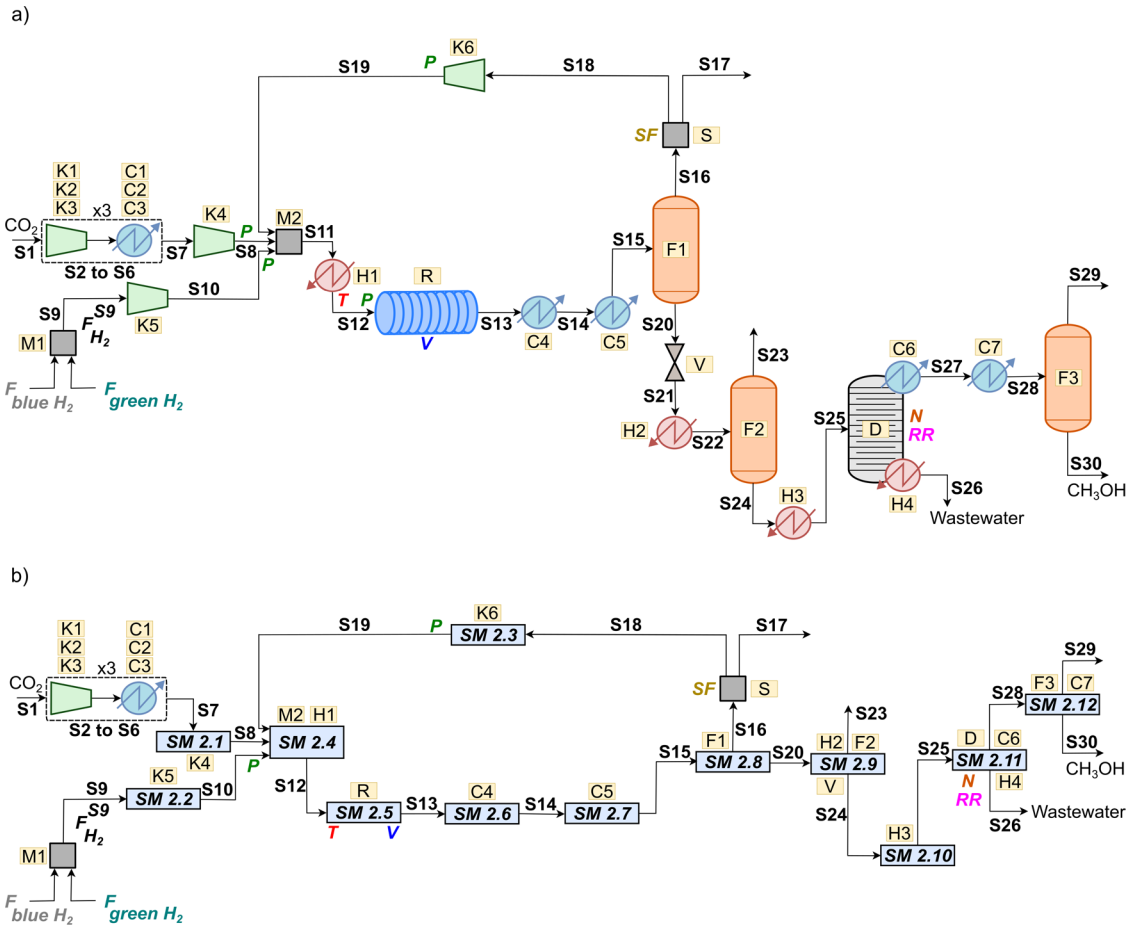

Degrees of freedom of the flowsheet					
$F_{blue\ H_2}$	Molar flow rate of blue H_2	*T*	Reaction temperature	*N*	Number of stages
$F_{green\ H_2}$	Molar flow rate of green H_2	*V*	PFR volume	*RR*	Reflux ratio
P	Reaction pressure	*SF*	Split fraction		

Figure 3. (a) Process flowsheet for methanol production. (b) Process flowsheet showing the process units replaced by surrogate models SM 2.1–SM 2.12. These process flowsheets have been adapted from our previous work.[37]

v3.7. For the bi-objective optimization of the HY model, we use the solver BARON[53] v21.1.13 in GAMS v35.2.0. For the bi-objective optimization of the GA and to calculate the hypervolume indicator, we use the Python package pymoo[54] v0.6.1. For the GA, we connect the flowsheet in Aspen Plus v11 with Python v3.7 using the COM interface, through which the NSGA-II algorithm directly queries the simulation at each optimization iteration. To avoid convergence errors during the optimization, we penalize nonconverged iterations with a high value.

CASE STUDY

As mentioned previously, the CO_2 hydrogenation to methanol process is considered for the case study. In this section, we first describe the process flowsheet, and then the two objective functions used in this case study.

Process Flowsheet. The process flowsheet shown in Figure 3a is based on the works by Van-Dal and Bouallou[55] and Vázquez and Guillén-Gosálbez.[22] We consider carbon dioxide (CO_2) obtained from direct air capture (DAC) powered by natural gas and electricity from the current global mix (the CO_2 is obtained at 25 °C and 1 bar). Hydrogen (H_2) can be obtained from either a fossil route, a green route, or a combination of both routes. The fossil route is the steam methane reforming (SMR) of natural gas with carbon capture and storage (CCS), i.e., blue H_2, while the green route is wind energy-powered water splitting, i.e., green H_2. We assume that the DAC and hydrogen production facilities are integrated with the methanol plant, and thus, the system boundary of the foreground system is set on the methanol production process, as done in some previous works.[19,56,57] Therefore, CO_2 and H_2 are inputs to the process (they belong to the background system, which is not optimized), with their corresponding costs and environmental impacts treated as given values for the LCA and optimization.

The DAC CO_2, which enters at a constant molar flow rate of 2,000 kmol·h^{-1}, is compressed using a compression train with intermediate cooling to reach the desired pressure (*P*, which is a degree of freedom) at the reactor inlet. The total H_2 feed is assumed to be available at 30 bar pressure, with its molar flow

https://doi.org/10.1021/acs.iecr.4c03563
Ind. Eng. Chem. Res. 2025, 64, 2816−2830

rate ($F^{S9}_{H_2}$) being the sum of the molar flow rates of the H_2 obtained from the fossil and green routes ($F_{\text{blue } H_2}$ and $F_{\text{green } H_2}$, respectively, both being degrees of freedom). After being compressed to pressure P, the H_2 is mixed with CO_2 and recycle stream S19, which is fed into a process heater. This heated stream (S12), with its temperature T being a degree of freedom, enters the adiabatic plug flow reactor (PFR, whose volume V is a degree of freedom), in which the carbon monoxide (CO) hydrogenation reaction (R1) and water−gas shift reaction (R2) take place in the presence of a commercial Cu-ZnO-Al_2O_3 catalyst. Reactions R1 and R2 lead to the global reaction R3:

$$CO + 2H_2 \leftrightarrows CH_3OH \quad \text{(R1)}$$

$$CO_2 + H_2 \leftrightarrows CO + H_2O \quad \text{(R2)}$$

$$CO_2 + 3H_2 \leftrightarrows CH_3OH + H_2O \quad \text{(R3)}$$

The outlet stream from the reactor (S13) is cooled to 35 °C using two successive coolers, after which it is sent to the first flash, which recycles most of the unreacted CO, CO_2, and H_2 to the reactor. A small part of the recycle stream is purged (defined using the split fraction SF, which is a degree of freedom), while the liquid outlet of the flash (stream S20) is expanded to 2 bar. This stream is sent to the second flash and then to a distillation column. The reflux ratio RR and the number of stages N of the distillation column are degrees of freedom. Note that the number of stages in the column is the only integer variable considered in this work. The distillate stream of the column, containing mainly CH_3OH and CO_2 (with a 99.9% molar recovery of CH_3OH) is sent to the third flash, resulting in a 99.5% pure stream of CH_3OH at the bottom. The distillation column generates a wastewater stream at the bottom, which is treated at a separate facility.

We use the thermodynamic packages Peng−Robinson and NRTL in the simulation. For the utilities, we consider electricity obtained from the grid, cooling water (20−30 °C), and natural gas heating. Regarding heat integration for the HY model and GA, we calculate the minimum heating and cooling utilities' requirements. For the HY model, we use the simultaneous process optimization and heat integration approach developed by Duran and Grossmann,[58] as all temperatures and flow rates of process streams can be modeled as variables (to be optimized). However, for the GA (NSGA-II algorithm), the degrees of freedom values are sent to the Aspen Plus flowsheet during each optimization run, and the flowsheet is converged. Thus, after converging the flowsheet, the temperatures and flow rates of all process streams are fixed and heat integration is performed. Nevertheless, both methods are conceptually the same, since both compute the minimum heating and cooling utilities' requirements, which are subsequently used in the computation of the objective functions. Therefore, the objective functions also remain the same for both the HY model and GA. For heat integration, we consider a minimum temperature difference of 10 °C, and the following units: process heaters (H1 and H3), process coolers (C1 to C5), condenser (C6) and reboiler (H4) of the column D, and flashes F2 and F3 (for which we define a heater (H2) and cooler (C7) before flashes F2 and F3, respectively).

The degrees of freedom of this flowsheet and their associated ranges are shown in Table 1. Note that while the molar flow rates of $F_{\text{blue } H_2}$ and $F_{\text{green } H_2}$ can individually vary between 0 and 6,000 kmol·h^{-1}, their total flow rate must be between the lower and upper bounds of 4,500 and 6,000 kmol·hr^{-1}. This is because the DAC CO_2 has a constant molar flow rate of 2,000 kmol·h^{-1}, hence stoichiometrically requiring a certain amount of H_2 in the feed. Thus, there are two constraints on $F_{\text{blue } H_2}$ and $F_{\text{green } H_2}$, as shown in Equation 13 below:

$$F_{\text{blue } H_2} + F_{\text{green } H_2} \geq 4,500$$
$$F_{\text{blue } H_2} + F_{\text{green } H_2} \leq 6,000 \quad (13)$$

Figure 3b shows the flowsheet with the process units replaced by surrogate models (labeled SM 2.1 to SM 2.12, respectively). An important point to note here is that for the LHS to generate the training and test data sets, we only consider one degree of freedom for the H_2 flow rate, with lower and upper bounds of 4,500 and 6,000 kmol·h^{-1}, respectively. Later, we define two input streams in GAMS (one each for $F_{\text{blue } H_2}$ and $F_{\text{green } H_2}$), and we use a mass balance to model mixer M1. The recycle stream splitter S is also modeled via a mass balance. As the molar flow rate of DAC CO_2 is constant, we do not model the compressors K1−K3 and coolers C1−C3; instead we use their constant electricity requirements and heat duties, respectively, as parameters in the calculations.

Table 1. Degrees of Freedom for the Case Study

Degrees of freedom	Symbol	Unit	Lower bound	Upper bound
Molar flow rate of blue H_2	$F_{\text{blue } H_2}$	kmol·h^{-1}	0.00	6,000.00
Molar flow rate of green H_2	$F_{\text{green } H_2}$	kmol·h^{-1}	0.00	6,000.00
Inlet temperature to PFR	T	°C	180.00	240.00
Inlet pressure to PFR	P	bar	45.00	55.00
Volume of PFR	V	m^3	35.00	54.00
Split fraction	SF	-	1.00×10^{-3}	5.00×10^{-2}
Reflux ratio	RR	-	1.25	1.80
Number of stages	N	-	45.00	55.00

Calculation of Objective Functions. Specifically, for this case study, the first objective function (F_1), i.e., the unitary production cost (in \$·kg^{-1} of methanol) is defined as follows:

$$F_1 = \frac{C_{DAC\ CO_2} + C_{blue\ H_2} + C_{green\ H_2} + C_{CU} + C_{HU} + C_{Electricity} + C_{Wastewater}}{M} \quad (14)$$

where the costs (in \$·h^{-1}) are denoted by $C_{\text{DAC } CO_2}$ (DAC CO_2), $C_{\text{blue } H_2}$ (blue H_2), $C_{\text{green } H_2}$ (green H_2), C_{CU} (cooling water), C_{HU} (natural gas heating), $C_{Electricity}$ (grid electricity), and $C_{Wastewater}$ (wastewater treatment). M denotes the methanol production rate (in kg·h^{-1}). The cost parameters for the calculations have been obtained from our earlier work,[37] as described in Section A of the Supporting Information. Note that for simplicity, the CAPEX term has been omitted as the main contribution to the total cost is coming from the raw materials, as shown in Section H of the Supporting Information.

For the second objective function (F_2), the functional unit for the LCA is 1 kg of methanol and the scope of the analysis is cradle-to-gate. The downscaling factor α is obtained from Vázquez and Guillén-Gosálbez.[22] The impact (IMP_k) in each

https://doi.org/10.1021/acs.iecr.4c03563
Ind. Eng. Chem. Res. 2025, 64, 2816−2830

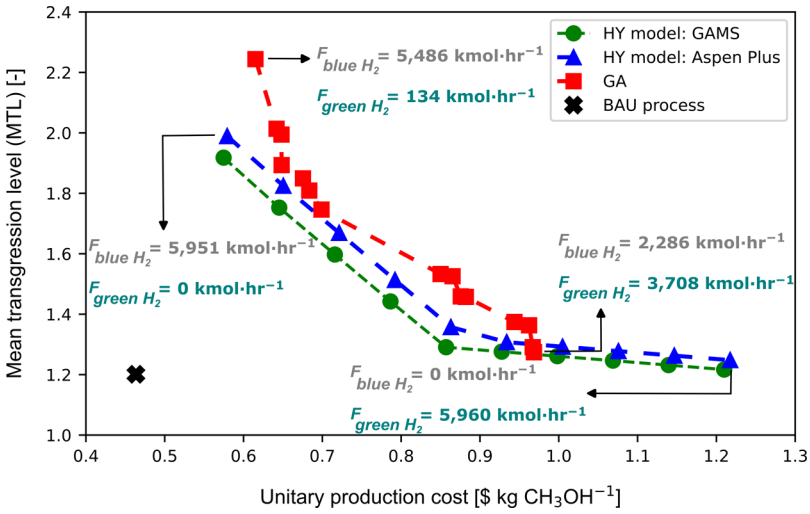

Figure 4. Pareto frontiers obtained from the bi-objective optimization of the HY model and GA. The unitary production cost for the BAU process has been obtained from Hank et al.,[61] while the MTL is calculated based on the data from the activity "methanol | methanol production | GLO" in the cutoff database of Ecoinvent v3.9.1.

impact category is defined as follows for the methanol production process:

$$\begin{aligned} IMP_k = {} & IMP_{k,DAC\ CO_2} + IMP_{k,blue\ H_2} + IMP_{k,green\ H_2} \\ & + IMP_{k,CU} + IMP_{k,HU} + IMP_{k,Electricity} + IMP_{k,Wastewater} \\ & + IMP_{k,Direct\ emissions} \quad \forall\, k \in K \end{aligned} \tag{15}$$

Here, $IMP_{k,DAC\ CO_2}$, $IMP_{k,blue\ H_2}$, $IMP_{k,green\ H_2}$, $IMP_{k,CU}$, $IMP_{k,HU}$, $IMP_{k,Electricity}$, $IMP_{k,Wastewater}$, and $IMP_{k,Direct\ emissions}$ refer to the impacts of DAC CO_2, blue H_2, green H_2, cooling utility, heating utility, grid electricity, wastewater treatment, and direct emissions, respectively for impact category k. As mentioned previously, these impacts are computed by connecting the mass and energy inputs from the technosphere to the foreground system (i.e., the Aspen Plus® simulation), with the corresponding life cycle impacts via eco vectors, which provide the life cycle impact per unit of reference flow using the cutoff database in Ecoinvent[59] v3.9.1 (retrieved using the Activity Browser[60] v2.10.1). For example, $IMP_{k,DAC\ CO_2}$ in Equation 15 is obtained as the product of the amount of DAC CO_2 consumed by the methanol production process and the impact per unit of DAC CO_2. The latter represents the product of the life cycle emissions per unit of DAC CO_2 and the corresponding characterization factors obtained from Ecoinvent v3.9.1. Further, the direct emissions include the emissions of CO_2, CO, H_2, CH_3OH, and H_2O from the three purge streams of the methanol process (streams S17, S23, and S29 in Figure 3), whose impact is determined from the product of the flow of these emissions and their respective characterization factors. Additional details of the parameters used to calculate the impacts are described in Section B of the Supporting Information.

Both models take the form of a mixed integer nonlinear programming (MINLP) problem. For the HY model, we chose a termination criterion of reaching a relative optimality gap of 1.00×10^{-9}, ensuring that the model is solved to global optimality within this tolerance. Note that this termination criterion does not apply to the GA since it is a derivative-free optimization technique. For the GA, we chose a maximum CPU time of 24,000 s as the termination criterion. As described in our previous work,[37] the BMS requires more time for model training, while the optimization is expected to be much faster due to the closed-form analytical equations generated. Specifically, the total training time for the HY model is 23,402 s in this case study, assuming parallelization of the BMS training step (i.e., assuming that all the BMS models are trained simultaneously). On the other hand, the GA does not have any training time (since there is no surrogate model created). Therefore, to ensure a fair comparison, we allow the GA to continue the optimization for a duration equivalent to the training plus optimization time of the HY model. We then chose a comparable time of 24,000 s as the termination criterion for the bi-objective optimization using the GA.

RESULTS AND DISCUSSION

In this section, we first compare the performances of the two optimization algorithms for the bi-objective optimization problem in terms of the Pareto frontiers obtained. Next, we show the environmental performance obtained from the best-performing algorithm (i.e., the HY model) for the current and prospective scenarios. Thus, in what follows, the optimal economic and environmental designs refer to the extreme points of the Pareto frontier obtained from the HY model. These designs are then compared to the BAU. We describe the uncertainty analysis for the LCA of the current scenario in Section F of the Supporting Information. This analysis is challenging for the prospective scenario, as future uncertainties in the life cycle inventories are not modeled in the *premise* database.[41]

Our results show that all single-objective process designs (BAU, optimal economic, and optimal environmental) transgress the SOS linked to the studied SDGs in at least one category, except for the optimal environmental design, which remains within the SOS relevant to SDG 13, i.e., climate action. Considering the prospective scenario, the overall performance of the studied processes improves significantly. Further details on these extreme designs and the Pareto alternatives are discussed next.

Results of the Bi-objective Optimization. Figure 4 shows the Pareto frontiers obtained from the bi-objective optimization using the HY model and GA, compared to the

https://doi.org/10.1021/acs.iecr.4c03563
Ind. Eng. Chem. Res. 2025, 64, 2816−2830

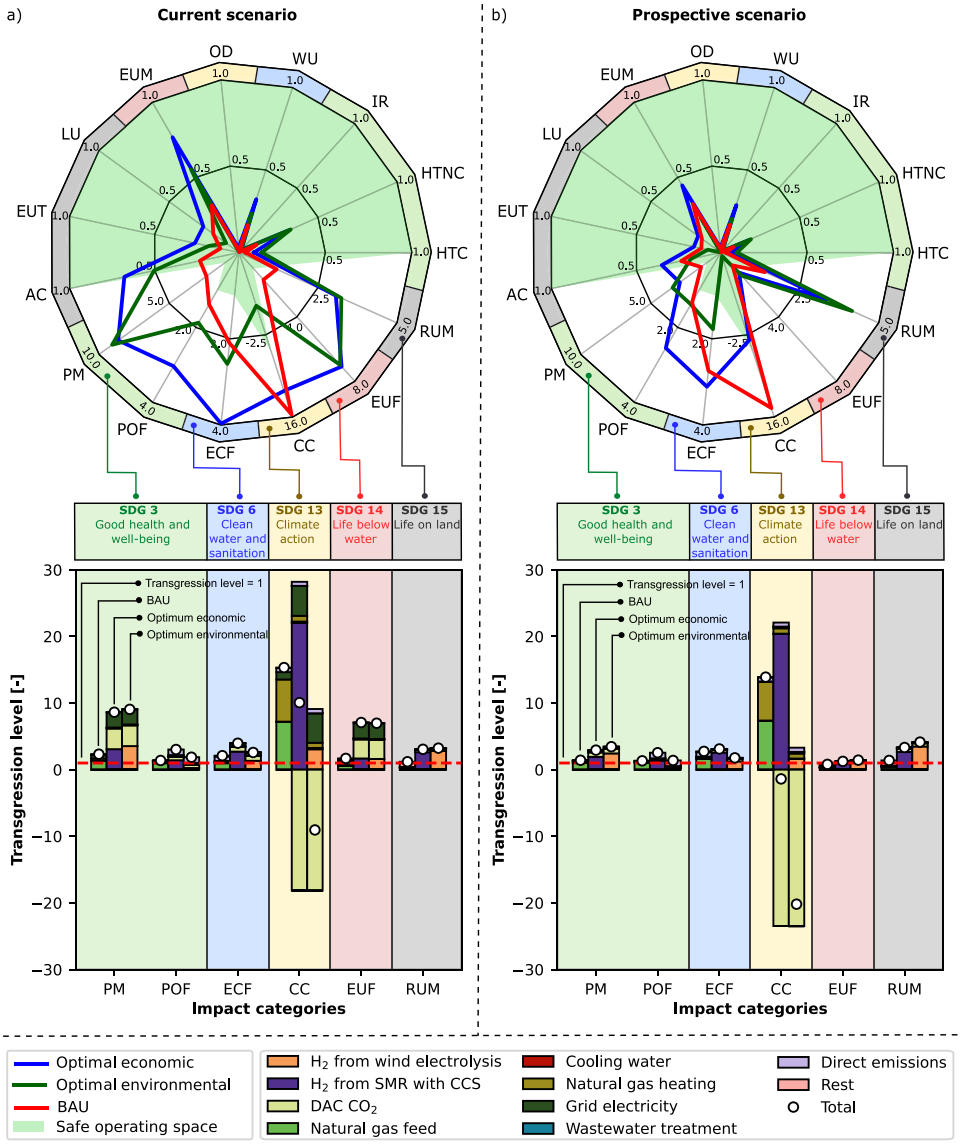

Figure 5. Transgression levels of impact categories and breakdown of transgression levels of impact categories lying outside the safe operating space for (a) current scenario and (b) prospective scenario. The abbreviations refer to the following impact categories - acidification (AC); eutrophication, terrestrial (EUT); land use (LU); eutrophication, marine (EUM); ozone depletion (OD); water use (WU); ionizing radiation (IR); human toxicity, noncarcinogenic (HTNC); human toxicity, carcinogenic (HTC); resource use, minerals and metals (RUM); eutrophication, freshwater (EUF); climate change (CC); ecotoxicity, freshwater (ECF); photochemical oxidant formation (POF); particulate matter (PM).

values of the objective functions for the BAU process. For the HY model, we show the Pareto frontiers based on the objective function values in GAMS as well as the actual objective function values from Aspen Plus. The GA optimization interacts with the Aspen Plus flowsheet, thus directly rendering the Pareto frontier.

The Pareto front obtained from the HY model's optimization dominates the one obtained from the GA's optimization. Taking the reference point (1.29, 2.31), we find that the hypervolume indicator for the HY model's Pareto front is 5.92×10^{-1} \$·kg^{-1}, while that of the GA's Pareto front is 5.43×10^{-1} \$·kg^{-1}, thus quantitively proving that the HY model performs better in the bi-objective optimization for a similar total CPU time (model building plus optimization).

Further, the HY model generated the Pareto frontier in 74 s (plus 23,402 s for model building), while the GA generated the Pareto frontier after the termination criterion of maximum time was reached (i.e., 26,672 s). Thus, the HY model, owing to the closed-form mathematical equations used as surrogate models, is able to find the global optimum of the surrogate model in a much shorter time compared to the GA. Moreover, the total training time and optimization time of the HY model is comparable to that of the GA. We find that the objective function values from GAMS are fairly close to those obtained from Aspen Plus for the HY model, with the percentage deviation for the MTL (2.41−4.91%) being higher than that for the unitary cost (0.62−0.79%). The higher deviation in the MTL is mainly due to differences in the heating utility obtained from GAMS and the actual values from Aspen Plus.

For both Pareto frontiers, we observe that the H_2 source is the major contributor to the objective functions' values. For the HY model, as we move from the minimum cost solution (optimal economic) to the minimum MTL (optimal environmental) solution, $F_{\text{blue H}_2}$ decreases from 5,951 to 0 kmol·h^{-1}, while $F_{\text{green H}_2}$ increases from 0 to 5,960 kmol·h^{-1}. For the GA

https://doi.org/10.1021/acs.iecr.4c03563
Ind. Eng. Chem. Res. 2025, 64, 2816−2830

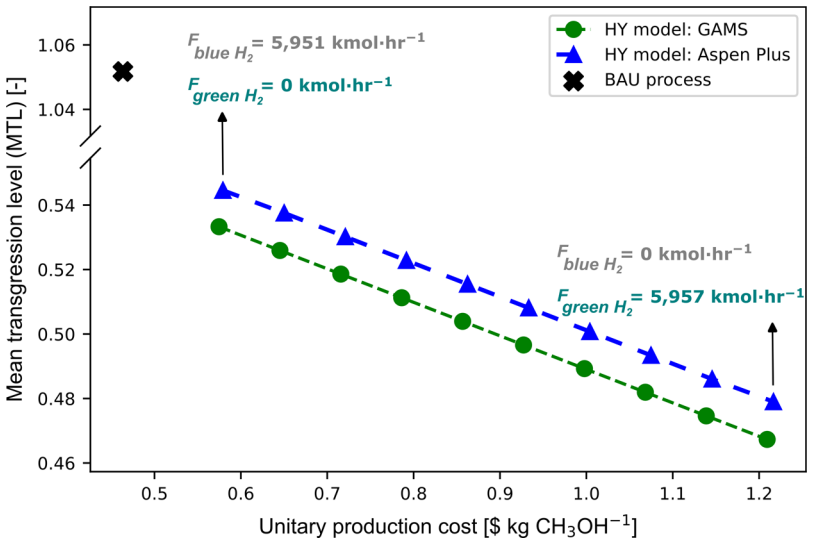

Figure 6. Pareto frontier obtained from the bi-objective optimization of the HY model for the prospective scenario.

model, $F_{\text{blue H}_2}$ decreases from 5,486 to 2,286 kmol·h^{-1}, while $F_{\text{green H}_2}$ increases from 134 to 3,708 kmol·h^{-1}. The intermediate Pareto points choose a hybridization between H_2 from both sources. This is because green H_2 has a higher cost, but an overall lower MTL compared to blue H_2.

Comparing the slopes of the two Pareto frontiers, we observe a linear Pareto frontier with a change in slope in one of the intermediate process designs for the HY model. This is because the operating conditions remain the same for all Pareto points except for minor changes in the minimum cost solution, and only the H_2 source changes as explained above. Moreover, at the intermediate point where the slope varies, the TL of climate change (which is one of the major contributors to the MTL until this point) drops below one, thus not contributing to the MTL thereafter. However, the share of the more expensive H_2 (i.e., green H_2) keeps increasing as it leads to a lower MTL (due to comparatively minor reductions in TLs of other impact categories). Therefore, for the remaining Pareto-optimal points, the increase in the unitary cost is relatively larger than the decrease in the MTL, hence leading to the observed shape of the Pareto frontier. However, for the GA, there is a significant variation in all operating conditions for different points of the Pareto frontier, thus resulting in a nonlinear front. Moreover, since we use the ϵ-constraint method for the HY model, the points on the Pareto frontier are (comparatively) equally spaced, which is not the case for the GA as it finds all nondominated points in a single optimization run using NSGA-II. Additional details of the optimization of the HY model and GA are shown in Section D of the Supporting Information.

Moreover, comparing the BAU process with the CO_2 hydrogenation process, we find that even the optimal economic performance of the CO_2 hydrogenation process has a higher cost than that of the BAU process. The primary reason for this behavior is that the BAU process uses syngas with an H_2/CO ratio of two. However, the CO_2 hydrogenation process uses more expensive DAC CO_2 and takes fossil H_2 from the same source as the BAU (i.e., SMR of natural gas), making the process comparatively less efficient as the H_2/CO_2 ratio increases to three (i.e., requiring 50% more H_2 than the BAU). Further, the cost goes on increasing as we move toward the optimal environmental performance, as green H_2 is more expensive than blue H_2.

Environmental Performance. As GA performs worse than the HY model in the bi-objective optimization, the results obtained from GA are not discussed in further detail. As described in the Methodology, it is important to note that the results discussed hereafter are based on the utilitarian downscaling of the SOS. Moreover, it should be noted that the SOS linked to an SDG is transgressed even if the SOS of only one impact category relevant to that SDG is transgressed, following the works by Ioannou et al.[25] and Negri et al.[62]

Current Scenario. As seen in Figure 5a, none of the methanol process designs are within the SOS linked to any of the studied SDGs, except for the optimal environmental design which stays within the SOS associated with SDG 13 (climate action). This is because at least one impact category linked to each SDG is transgressed by all process designs. Specifically, the SOS linked to SDG 3 is transgressed by the particulate matter and photochemical oxidant formation impact categories, while SDGs 6, 13, 14, and 15 are affected by transgressions of freshwater ecotoxicity, climate change, freshwater eutrophication, and material resource use, respectively. Regarding SDG 13, the optimal environmental design does not transgress the share of the SOS due to the use of captured CO_2 and electrolytic H_2 from wind power. Moreover, the transgression of the optimal environmental design is negative as we adopt a cradle-to-gate scope, subtracting from the life cycle CO_2 emissions the CO_2 contribution from the DAC.

Regarding the aggregated environmental performance variable, i.e., the MTL, we obtain values for the BAU process, optimal economic, and optimal environmental designs of 1.20, 1.99, and 1.25, respectively, which is due to the occurrence of burden shifting (i.e., despite a better performance in the climate change category, the MTL of the CO_2 hydrogenation process is worse than that of the BAU). More specifically, compared to the BAU process, particulate matter, freshwater eutrophication, and material resource use worsen the most for the two CO_2 hydrogenation process designs. This affects the other SDGs for these two designs, despite greatly improving SDG 13 (climate action) compared with the BAU process. The H_2 sources (both blue and green), DAC CO_2, and grid

https://doi.org/10.1021/acs.iecr.4c03563
Ind. Eng. Chem. Res. 2025, 64, 2816−2830

electricity are the major contributors to the burden-shifting to these three categories. The primary cause of the burden shifting for green H_2 is the impact originating from the construction of wind turbines. For blue H_2, most of the impact comes from the natural gas feed and the infrastructure, while for DAC CO_2, it comes from grid electricity.

Considering the breakdown of the TLs, most of the impact in the BAU process comes from natural gas (i.e., both as a feedstock and heating utility) and grid electricity. In the optimal economic design, the feedstock (DAC CO_2 and blue H_2), and grid electricity represent most of the impact across all categories, while the DAC CO_2 reduces climate change (i.e., appears as a negative contribution) due to the removal of CO_2 from the atmosphere. The optimal environmental design follows the same trend as the optimal economic design, where the impact from blue H_2 is replaced by that of green H_2 (as the H_2 feed share from water electrolysis gradually increases from 0 to 100% as we go from the optimal economic design to the optimal environmental design).

Note that the other impact categories within the SOS are discussed in Section E of the Supporting Information. We next conduct a prospective LCA for the year 2050, to analyze the impact of process improvements in the BAU as well as in CO_2 hydrogenation in the future.

Prospective Scenario. The Pareto front obtained from the optimization of the HY model is shown in Figure 6, with the numerical results shown in Section D of the Supporting Information.

As seen in the previous section, the H_2 source dominates the objective function evaluations. As we move from the minimum cost solution to the minimum MTL solution in Figure 6, $F_{\text{blue H}_2}$ decreases from 5,951 to 0 kmol·h^{-1}, while $F_{\text{green H}_2}$ increases from 0 to 5,957 kmol·h^{-1}. The intermediate Pareto points choose a hybridization between H_2 from both sources. Following the same approach as the LCA results for the current scenario, the impact of all designs on the SDGs and the MTL is discussed next, with the results shown in Figure 5b.

Here, in contrast to the current scenario, the BAU process does not transgress the SOS linked to SDG 14, while both the optimal economic and environmental designs do not transgress the SOS relevant to SDG 13. The overall improvement in the TLEs in the prospective scenario lies between 41 and 93% in the optimal environmental design, yet it is still not sufficient to lie within the SOS of the other SDGs. The only categories worsening in the prospective scenario are material resource use (for all three designs) and freshwater ecotoxicity (for the BAU).

Next, comparing the MTL of the BAU, optimal economic, and optimal environmental processes in 2050 (1.05, 0.55, and 0.48, respectively), we observe a substantial decrease (12, 73, and 62%, respectively) relative to the current scenario. Therefore, in 2050, the optimal environmental design of the CO_2 hydrogenation process is expected to show the best overall environmental performance. However, burden-shifting due to the use of blue and green H_2 is still relevant (Figure 5b), while the contribution of DAC CO_2 and grid electricity drops substantially (due to the decarbonization of the electricity mix). This results in a 110% decrease in the TL of climate change in the optimal economic design (TL = −1.38) compared to the BAU (TL = 13.90), which was only 34% lower in the current scenario. The optimal environmental design shows a 245% decrease (TL = −20.19) compared to the BAU. Nonetheless, the BAU still has a lower TL than the CO_2 hydrogenation process designs in the particulate matter, freshwater eutrophication, and material resource use categories. However, the percentage difference is substantially lower than that in the current scenario (except for the material resource use category), which eventually results in a much lower MTL for the CO_2 hydrogenation process.

Finally, the breakdown of the TLs shows that a majority of the impact in the BAU process still comes from natural gas (i.e., both as a feedstock and as a heating utility), which is not expected to show major process improvements in 2050. However, the contribution of grid electricity decreases substantially, due to the expected decarbonization of the electricity mix. A similar trend is seen for the optimal economic and environmental designs, where the H_2 feedstocks together contribute a majority of the impact across all categories. The decarbonization of the electricity mix also results in a larger negative contribution of DAC CO_2 in the climate change impact category.

CONCLUSIONS

In this work, we developed a framework for the optimal design of chemical processes aligned with the SDGs. More specifically, we embedded SDGs-based absolute sustainability criteria in a hybrid analytical surrogate process model constructed using Bayesian symbolic regression. As objective functions, we optimized the unitary production cost and the mean transgression level, defined using maximum impact thresholds that should not be exceeded and which are contextualized using the SDGs and the PBs framework.

First, comparing with a multiobjective derivative-free optimization algorithm (i.e., NSGA-II) using methanol production as a test bed, we found that the optimization of the hybrid model generates a Pareto frontier which dominates the one found using the derivative-free optimization algorithm (for the same total CPU time in both methods). Thus, the longer training time of the hybrid model is offset by its substantially better optimization performance.

Moreover, our analysis reveals that, at present, all process designs transgress the SOS linked to the PBs associated with the five SDGs studied here (i.e., SDGs 3, 6, 13, 14, and 15), except for the optimal environmental design that would be consistent with SDG 13, i.e., climate action. However, there would be burden shifting from climate change mainly to three other impact categories (particulate matter, freshwater eutrophication, and material resource use). This collateral damage caused when shifting to green methanol would be much less relevant in the future according to our prospective LCA. We note that these conclusions are based on the utilitarian downscaling principle, which is not exempt from limitations. Moreover, the mean transgression level could be defined in alternative ways, avoiding equal weights for all impacts and instead prioritizing some of them. These methodological changes would then lead to different results. We should also note that not all metrics are affected by uncertainties in the same manner, which should also be considered in the interpretation of the results. Acknowledging these limitations, we still believe that analyzing impacts beyond climate change, contextualized using absolute thresholds, provides very valuable insights into the process design problem.

Overall, our work showcases the opportunities of including SDG criteria in process design along with the advantages of

https://doi.org/10.1021/acs.iecr.4c03563
Ind. Eng. Chem. Res. 2025, 64, 2816−2830

using hybrid analytical surrogate models to generate the corresponding Pareto solutions. Future work could include additional sustainability assessment metrics, as well as other downscaling approaches, to generate further insights into the problem. Applications to other case studies will also be another research direction worthy of pursuing.

■ ASSOCIATED CONTENT

Supporting Information

The Supporting Information is available free of charge at https://pubs.acs.org/doi/10.1021/acs.iecr.4c03563.

> Data for the economic evaluation (Section A), environmental evaluation (Section B), additional details of the surrogate modeling (Section C), additional results of the bi-objective optimization (Section D), additional results related to the environmental performance (Section E), uncertainty analysis for the life cycle assessment (Section F), additional comments specifically on the use of DAC CO_2 (Section G), and sizing and costing analysis of the methanol plant equipment (Section H) (PDF)

■ AUTHOR INFORMATION

Corresponding Author

Gonzalo Guillén-Gosálbez − *Institute for Chemical and Bioengineering, Department of Chemistry and Applied Biosciences, ETH Zurich, 8093 Zurich, Switzerland;* orcid.org/0000-0001-6074-8473; Email: gonzalo.guillen.gosalbez@chem.ethz.ch

Authors

Sachin Jog − *Institute for Chemical and Bioengineering, Department of Chemistry and Applied Biosciences, ETH Zurich, 8093 Zurich, Switzerland;* orcid.org/0000-0003-3927-4036

Daniel Vázquez − *IQS School of Engineering, Universitat Ramon Llull, 08017 Barcelona, Spain;* orcid.org/0000-0001-9380-3918

Lucas F. Santos − *Institute for Chemical and Bioengineering, Department of Chemistry and Applied Biosciences, ETH Zurich, 8093 Zurich, Switzerland*

Juan D. Medrano-García − *Institute for Chemical and Bioengineering, Department of Chemistry and Applied Biosciences, ETH Zurich, 8093 Zurich, Switzerland;* orcid.org/0000-0001-5422-1683

Complete contact information is available at: https://pubs.acs.org/10.1021/acs.iecr.4c03563

Author Contributions

The manuscript was written through contributions of all authors. All authors have given approval to the final version of the manuscript.

Funding

The authors would like to acknowledge the financial support from the Swiss National Science Foundation (Project LEARN-D, MINT 200021_214877). D.V. and J.D.M-G. acknowledge support from grant PID2023-151826OA-I00 funded by MICIU/AEI/ 10.13039/501100011033 and ERDF/EU.

Notes

The authors declare no competing financial interest.

■ ACKNOWLEDGMENTS

The authors would like to acknowledge the financial support from the Swiss National Science Foundation (Project LEARN-D, MINT 200021_214877). D.V. and J.D.M-G. acknowledge support from grant PID2023-151826OA-I00 funded by MICIU/AEI/ 10.13039/501100011033 and ERDF/EU.

■ ABBREVIATIONS

ANN	artificial neural network
BAU	business-as-usual
BMS	Bayesian machine scientist
CCS	carbon capture and storage
CCU	carbon capture and utilization
DAC	direct air capture
EF	environmental footprint
EU	European Union
GA	Genetic algorithm
GVA	gross value added
HY	Hybrid
IAM	integrated assessment model
IMAGE	integrated model to assess the global environment
LCA	life cycle assessment
LCI	life cycle inventory
LCO	life cycle optimization
LHS	Latin hypercube sampling
LP	linear programming
MAPE	mean absolute percentage error
MCMC	Markov chain Monte Carlo
MINLP	mixed integer nonlinear programming
MSE	mean squared error
MTL	mean transgression level
NSGA	nondominated sorting genetic algorithm
OPEX	operating expenditures
PB	planetary boundary
PFR	plug flow reactor
PSE	process systems engineering
RCP	Representative concentration pathway
SDG	sustainable development goal
SMR	steam methane reforming
SSP	shared socio-economic pathway
SOS	safe operating space
TL	transgression level
TLE	transgression level excess
UN	United Nations
VEGA	vector evaluated genetic algorithm

■ SUBSCRIPTS

$i \in I$	process units replaced with a surrogate
$j \in J$	surrogate process models
$j \in JI_i \subset J$	each surrogate model j of each process unit i
$c \in C$	continuous process variables
$u \in U$	continuous structural variables
$z \in Z$	integer variables
$c \in IM_{ij}^{C} \subset C$	continuous process variables used as inputs for process unit i and model j
$u \in IM_{ij}^{U} \subset U$	continuous structural variables used as inputs for process unit i and model j
$z \in IM_{ij}^{Z} \subset Z$	integer variables used as inputs for process unit i and model j
$c \in OM_{ij}^{C} \subset C$	continuous process variables obtained as outputs from process unit i and model j
$m \in M$	life cycle inventory entries

https://doi.org/10.1021/acs.iecr.4c03563
Ind. Eng. Chem. Res. 2025, 64, 2816−2830

$r \in R$	raw materials
$t \in T$	utilities
$k \in K$	impact categories

PARAMETERS

α	downscaling factor
ε	parameter in the epsilon constraint method
$CF_{k,m}$	characterization factor of LCI entry m for impact category k
LCI_m	life cycle inventory of LCI entry m
SOS_k	safe operating space for impact category k

VARIABLES

x	continuous variable
z	integer variable
c	continuous process variable
u	continuous structural variable
x_c	value of continuous process variable
d_u	value of continuous structural variable
y_z	value of integer variable
F_1	value of first objective function
F_2	value of second objective function
f_1^{HY}	value of first objective function from the hybrid model
f_2^{HY}	value of second objective function from the hybrid model
D_1	percentage deviation between surrogate and actual values of first objective function
D_2	percentage deviation between surrogate and actual values of second objective function
$F_{blue\ H_2}$	molar flow rate of blue H_2 [kmol·h^{-1}]
$F_{green\ H_2}$	molar flow rate of green H_2 [kmol·h^{-1}]
T	plug flow reactor inlet temperature [°C]
P	plug flow reactor inlet pressure [bar]
V	plug flow reactor volume [m^3]
SF	split fraction
RR	reflux ratio
N	number of stages
$C_{DAC\ CO_2}$	cost of direct air captured CO_2 [$·h^{-1}]
$C_{blue\ H_2}$	cost of blue H_2 [$·h^{-1}]
$C_{green\ H_2}$	cost of green H_2 [$·h^{-1}]
C_{CU}	cost of cooling utility [$·h^{-1}]
C_{HU}	cost of heating utility [$·h^{-1}]
$C_{Electricity}$	cost of grid electricity [$·h^{-1}]
$C_{Wastewater}$	cost of wastewater treatment [$·h^{-1}]
M	methanol production rate [kg·h^{-1}]
IMP_k	total impact of impact category k
$IMP_{k,DAC\ CO_2}$	impact of DAC CO_2 for impact category k
$IMP_{k,blue\ H_2}$	impact of blue H_2 for impact category k
$IMP_{k,green\ H_2}$	impact of green H_2 for impact category k
$IMP_{k,CU}$	impact of cooling utility for impact category k
$IMP_{k,HU}$	impact of heating utility for impact category k
$IMP_{k,Electricity}$	impact of grid electricity for impact category k
$IMP_{k,Wastewater}$	impact of wastewater treatment for impact category k
$IMP_{k,Direct\ emissions}$	impact of direct emissions for impact category k
TL_k	transgression level of impact category k
TLE_k	transgression level excess of impact category k

REFERENCES

(1) United Nations. *Framework Convention on Climate Change (UNFCCC), Paris Agreement; United Nations*. 2016. https://unfccc.int/process-and-meetings/the-paris-agreement/the-paris-agreement (accessed June 2024).

(2) Bauer, F.; Tilsted, J. P.; Pfister, S.; Oberschelp, C.; Kulionis, V. Mapping GHG Emissions and Prospects for Renewable Energy in the Chemical Industry. *Curr. Opin. Chem. Eng.* **2023**, *39*, 100881.

(3) Guillén-Gosálbez, G.; You, F.; Galán-Martín, Á.; Pozo, C.; Grossmann, I. E. Process Systems Engineering Thinking and Tools Applied to Sustainability Problems: Current Landscape and Future Opportunities. *Curr. Opin. Chem. Eng.* **2019**, *26*, 170−179.

(4) Huijbregts, M. A. J.; Steinmann, Z. J. N.; Elshout, P. M. F.; Stam, G.; Verones, F.; Vieira, M.; Zijp, M.; Hollander, A.; van Zelm, R. ReCiPe2016: A Harmonised Life Cycle Impact Assessment Method at Midpoint and Endpoint Level. *Int. J. Life Cycle Assess.* **2017**, *22* (2), 138−147.

(5) Jolliet, O.; Margni, M.; Charles, R.; Humbert, S.; Payet, J.; Rebitzer, G.; Rosenbaum, R. IMPACT 2002+: A New Life Cycle Impact Assessment Methodology. *Int. J. Life Cycle Assess.* **2003**, *8* (6), 324.

(6) European Commission (EC). *PEFCR Guidance Document - Guidance for the Development of Product Environmental Footprint Category Rules (PEFCRs), version 6.3*; European Commission, 2017. http://ec.europa.eu/environment/eussd/smgp/pdf/PEFCR_guidance_v6.3.pdf (accessed July 2024).

(7) Azapagic, A.; Clift, R. Life Cycle Assessment and Multiobjective Optimisation. *J. Clean. Prod.* **1999**, *7* (2), 135−143.

(8) Mele, F. D.; Guillén-Gosálbez, G.; Jiménez, L. Optimal Planning of Supply Chains for Bioethanol and Sugar Production with Economic and Environmental Concerns. *In Computer Aided Chemical Engineering* **2009**, *26*, 997−1002.

(9) Zamboni, A.; Bezzo, F.; Shah, N. Spatially Explicit Static Model for the Strategic Design of Future Bioethanol Production Systems. 2. Multi-Objective Environmental Optimization. *Energy Fuels* **2009**, *23* (10), 5134−5143.

(10) You, F.; Wang, B. Life Cycle Optimization of Biomass-to-Liquid Supply Chains with Distributed−Centralized Processing Networks. *Ind. Eng. Chem. Res.* **2011**, *50* (17), 10102−10127.

(11) Elia, J. A.; Baliban, R. C.; Xiao, X.; Floudas, C. A. Optimal Energy Supply Network Determination and Life Cycle Analysis for Hybrid Coal, Biomass, and Natural Gas to Liquid (CBGTL) Plants Using Carbon-Based Hydrogen Production. *Comput. Chem. Eng.* **2011**, *35* (8), 1399−1430.

(12) Alexander, B.; Barton, G.; Petrie, J.; Romagnoli, J. Process Synthesis and Optimisation Tools for Environmental Design: Methodology and Structure. *Comput. Chem. Eng.* **2000**, *24* (2−7), 1195−1200.

(13) Fu, Y.; Diwekar, U. M.; Young, D.; Cabezas, H. Process Design for the Environment: A Multi-Objective Framework under Uncertainty. *Clean Prod. Process.* **2000**, *2* (2), 0092−0107.

(14) Guillén-Gosálbez, G.; Caballero, J. A.; Esteller, L. J.; Gadalla, M. Application of Life Cycle Assessment to the Structural Optimization of Process Flowsheets. *In Computer Aided Chemical Engineering* **2007**, *24*, 1163−1168.

(15) Boyce, J.; Sacchi, R.; Goetheer, E.; Steubing, B. A Prospective Life Cycle Assessment of Global Ammonia Decarbonisation Scenarios. *Heliyon* **2024**, *10* (6), e27547.

(16) Nabera, A.; José Martín, A.; Istrate, R.; Pérez-Ramírez, J.; Guillén-Gosálbez, G. Integrating Climate Policies in the Sustainability Analysis of Green Chemicals. *Green Chem.* **2024**, *26* (11), 6461−6469.

(17) Rockström, J.; Steffen, W.; Noone, K.; Persson, Å.; Chapin, F. S.; Lambin, E. F.; Lenton, T. M.; Scheffer, M.; Folke, C.; Schellnhuber, H. J.; Nykvist, B.; de Wit, C. A.; Hughes, T.; van der Leeuw, S.; Rodhe, H.; Sörlin, S.; Snyder, P. K.; Costanza, R.; Svedin,

https://doi.org/10.1021/acs.iecr.4c03563
Ind. Eng. Chem. Res. 2025, 64, 2816−2830

U.; Falkenmark, M.; Karlberg, L.; Corell, R. W.; Fabry, V. J.; Hansen, J.; Walker, B.; Liverman, D.; Richardson, K.; Crutzen, P.; Foley, J. A. A Safe Operating Space for Humanity. *Nature* **2009**, *461* (7263), 472−475.
(18) Steffen, W.; Richardson, K.; Rockström, J.; Cornell, S. E.; Fetzer, I.; Bennett, E. M.; Biggs, R.; Carpenter, S. R.; de Vries, W.; de Wit, C. A.; Folke, C.; Gerten, D.; Heinke, J.; Mace, G. M.; Persson, L. M.; Ramanathan, V.; Reyers, B.; Sörlin, S. Planetary Boundaries: Guiding Human Development on a Changing Planet. *Science (80-.).* **2015**, *347* (6223). .
(19) González-Garay, A.; Frei, M. S.; Al-Qahtani, A.; Mondelli, C.; Guillén-Gosálbez, G.; Pérez-Ramírez, J. Plant-to-Planet Analysis of CO_2-Based Methanol Processes. *Energy Environ. Sci.* **2019**, *12* (12), 3425−3436.
(20) Algunaibet, I. M.; Pozo, C.; Galán-Martín, Á.; Huijbregts, M. A. J.; Mac Dowell, N.; Guillén-Gosálbez, G. Powering Sustainable Development within Planetary Boundaries. *Energy Environ. Sci.* **2019**, *12* (6), 1890−1900.
(21) Ehrenstein, M.; Galán-Martín, Á.; Tulus, V.; Guillén-Gosálbez, G. Optimising Fuel Supply Chains within Planetary Boundaries: A Case Study of Hydrogen for Road Transport in the UK. *Appl. Energy* **2020**, *276*, 115486.
(22) Vázquez, D.; Guillén-Gosálbez, G. Process Design within Planetary Boundaries: Application to CO_2 Based Methanol Production. *Chem. Eng. Sci.* **2021**, *246*, 116891.
(23) United Nations (UN). *Sustainable development goals*; 2015. https://sdgs.un.org/ (accessed July 2024).
(24) Sala, S.; Crenna, E.; Secchi, M.; Sanyé-Mengual, E. Environmental Sustainability of European Production and Consumption Assessed against Planetary Boundaries. *J. Environ. Manage.* **2020**, *269*, 110686.
(25) Ioannou, I.; Galán-Martín, Á.; Pérez-Ramírez, J.; Guillén-Gosálbez, G. Trade-Offs between Sustainable Development Goals in Carbon Capture and Utilisation. *Energy Environ. Sci.* **2023**, *16* (1), 113−124.
(26) Wolday, A. K.; Ramteke, M. Surrogate Model-Based Optimization of Methanol Synthesis Process for Multiple Objectives: A Pathway towards Achieving Sustainable Development Goals. *Chem. Eng. Res. Des.* **2024**, *204*, 172−182.
(27) Koza, J. R. *Genetic Programming: On the Programming of Computers by Means of Natural Selection*; MIT Press: Cambridge, 1992.
(28) Orzechowski, P.; Moore, J. H. Where Are We Now? A Large Benchmark Study of Recent Symbolic Regression Methods. In *GECCO 2018 - Proceedings of the 2018 Genetic and Evolutionary Computation Conference*; Association for Computing Machinery, Inc., 2018; pp 1183−1190.
(29) Cozad, A.; Sahinidis, N. V. A Global MINLP Approach to Symbolic Regression. *Math. Program.* **2018**, *170* (1), 97−119.
(30) Guimerà, R.; Reichardt, I.; Aguilar-Mogas, A.; Massucci, F. A.; Miranda, M.; Pallarès, J.; Sales-Pardo, M. A Bayesian Machine Scientist to Aid in the Solution of Challenging Scientific Problems. *Sci. Adv.* **2020**, *6* (5). .
(31) Forster, T.; Vázquez, D.; Guillén-Gosálbez, G. Algebraic Surrogate-based Process Optimization Using Bayesian Symbolic Learning. *AIChE J.* **2023**.
(32) Psichogios, D. C.; Ungar, L. H. A Hybrid Neural Network-First Principles Approach to Process Modeling. *AIChE J.* **1992**, *38* (10), 1499−1511.
(33) Henao, C. A.; Maravelias, C. T. Surrogate-Based Superstructure Optimization Framework. *AIChE J.* **2011**, *57* (5), 1216−1232.
(34) Fahmi, I.; Cremaschi, S. Process Synthesis of Biodiesel Production Plant Using Artificial Neural Networks as the Surrogate Models. *Comput. Chem. Eng.* **2012**, *46*, 105−123.
(35) Quirante, N.; Caballero, J. A. Large Scale Optimization of a Sour Water Stripping Plant Using Surrogate Models. *Comput. Chem. Eng.* **2016**, *92*, 143−162.
(36) Quirante, N.; Javaloyes-Antón, J.; Caballero, J. A. Hybrid Simulation-Equation Based Synthesis of Chemical Processes. *Chem. Eng. Res. Des.* **2018**, *132*, 766−784.
(37) Jog, S.; Vázquez, D.; Santos, L. F.; Caballero, J. A.; Guillén-Gosálbez, G. Hybrid Analytical Surrogate-Based Process Optimization via Bayesian Symbolic Regression. *Comput. Chem. Eng.* **2024**, *182*, 108563.
(38) Mesquita-Cunha, M.; Figueira, J. R.; Barbosa-Póvoa, A. P. New ϵ-Constraint Methods for Bi-objective Integer Linear Programming: A Pareto Front Representation Approach. *Eur. J. Oper. Res.* **2023**, *306* (1), 286−307.
(39) Hjalsted, A. W.; Laurent, A.; Andersen, M. M.; Olsen, K. H.; Ryberg, M.; Hauschild, M. Sharing the Safe Operating Space: Exploring Ethical Allocation Principles to Operationalize the Planetary Boundaries and Assess Absolute Sustainability at Individual and Industrial Sector Levels. *J. Ind. Ecol.* **2021**, *25* (1), 6−19.
(40) D'Angelo, S. C.; Cobo, S.; Tulus, V.; Nabera, A.; Martín, A. J.; Pérez-Ramírez, J.; Guillén-Gosálbez, G. Planetary Boundaries Analysis of Low-Carbon Ammonia Production Routes. *ACS Sustain. Chem. Eng.* **2021**, *9* (29), 9740−9749.
(41) Salah, C.; Istrate, R.; Bjørn, A.; Tulus, V.; Pérez-Ramírez, J.; Guillén-Gosálbez, G. Environmental Benefits of Circular Ethylene Production from Polymer Waste. *ACS Sustainable Chem. Eng.* **2024**, *12*, 13897−13906.
(42) Ryberg, M. W.; Andersen, M. M.; Owsianiak, M.; Hauschild, M. Z. Downscaling the Planetary Boundaries in Absolute Environmental Sustainability Assessments−A Review. *J. Clean. Prod.* **2020**, *276*, 123287.
(43) Bos, U.; Horn, R.; Beck, T.; Lindner, J. P.; Fischer, M. *LANCA - Characterization Factors for Life Cycle Impact Assessment - Version 2.0*; Fraunhofer Inst., 2016; p 166.
(44) *Integrated Assessment of Global Environmental Change with IMAGE 3.0*; PBL Netherlands Environmental Assessment Agency, 2014.
(45) Sacchi, R.; Terlouw, T.; Siala, K.; Dirnaichner, A.; Bauer, C.; Cox, B.; Mutel, C.; Daioglou, V.; Luderer, G. PRospective EnvironMental Impact AsSEment (Premise): A Streamlined Approach to Producing Databases for Prospective Life Cycle Assessment Using Integrated Assessment Models. *Renew. Sustain. Energy Rev.* **2022**, *160*, 112311.
(46) Mavrotas, G. Effective Implementation of the ϵ-Constraint Method in Multi-Objective Mathematical Programming Problems. *Appl. Math. Comput.* **2009**, *213* (2), 455−465.
(47) Zitzler, E.; Thiele, L. Multiobjective Optimization Using Evolutionary Algorithms — A Comparative Case Study. *In Lecture Notes in Computer Science* **1998**, *1498*, 292−301.
(48) Schaffer, J. D. *Some Experiments in Machine Learning Using Vector Evaluated Genetic Algorithms*; Vanderbilt Univ.: Nashville, TN, 1985.
(49) Srinivas, N.; Deb, K. Muiltiobjective Optimization Using Nondominated Sorting in Genetic Algorithms. *Evol. Comput.* **1994**, *2* (3), 221−248.
(50) Deb, K.; Pratap, A.; Agarwal, S.; Meyarivan, T. A Fast and Elitist Multiobjective Genetic Algorithm: NSGA-II. *IEEE Trans. Evol. Comput.* **2002**, *6* (2), 182−197.
(51) Goldberg, D. E. *Genetic Algorithms in Search, Optimization and Machine Learning*; Addison-Wesley: Reading, MA, 1989.
(52) Ishibuchi, H.; Imada, R.; Setoguchi, Y.; Nojima, Y. Reference Point Specification in Hypervolume Calculation for Fair Comparison and Efficient Search. In *Proceedings of the Genetic and Evolutionary Computation Conference*; ACM: New York, NY, 2017; pp 585−592.
(53) Tawarmalani, M.; Sahinidis, N. V. A Polyhedral Branch-and-Cut Approach to Global Optimization. *Math. Program.* **2005**, *103* (2), 225−249.
(54) Blank, J.; Deb, K. Pymoo: Multi-Objective Optimization in Python. *IEEE Access* **2020**, *8*, 89497−89509.
(55) Van-Dal, É. S.; Bouallou, C. Design and Simulation of a Methanol Production Plant from CO_2 Hydrogenation. *J. Clean. Prod.* **2013**, *57*, 38−45.

https://doi.org/10.1021/acs.iecr.4c03563
Ind. Eng. Chem. Res. 2025, 64, 2816−2830

(56) Pérez-Fortes, M.; Schöneberger, J. C.; Boulamanti, A.; Tzimas, E. Methanol Synthesis Using Captured CO_2 as Raw Material: Techno-Economic and Environmental Assessment. *Appl. Energy* **2016**, *161*, 718−732.
(57) Ioannou, I.; Javaloyes-Antón, J.; Caballero, J. A.; Guillén-Gosálbez, G. Economic and Environmental Performance of an Integrated CO_2 Refinery. *ACS Sustain. Chem. Eng.* **2023**, *11* (5), 1949−1961.
(58) Duran, M. A.; Grossmann, I. E. Simultaneous Optimization and Heat Integration of Chemical Processes. *AIChE J.* **1986**, *32* (1), 123−138.
(59) Wernet, G.; Bauer, C.; Steubing, B.; Reinhard, J.; Moreno-Ruiz, E.; Weidema, B. The Ecoinvent Database Version 3 (Part I): Overview and Methodology. *Int. J. Life Cycle Assess.* **2016**, *21* (9), 1218−1230.
(60) Steubing, B.; de Koning, D.; Haas, A.; Mutel, C. L. The Activity Browser — An Open Source LCA Software Building on Top of the Brightway Framework. *Softw. Impacts* **2020**, *3*, 100012.
(61) Hank, C.; Gelpke, S.; Schnabl, A.; White, R. J.; Full, J.; Wiebe, N.; Smolinka, T.; Schaadt, A.; Henning, H.-M.; Hebling, C. Economics & Carbon Dioxide Avoidance Cost of Methanol Production Based on Renewable Hydrogen and Recycled Carbon Dioxide−Power-to-Methanol. *Sustain. Energy Fuels* **2018**, *2* (6), 1244−1261.
(62) Negri, V.; Charalambous, M. A.; Medrano-García, J. D.; Guillén-Gosálbez, G. Sustainable Development Goals Assessment of Carbon Capture On-Board. *Comput. Aided Chem. Eng.* **2023**, *52*, 2929−2934.

https://doi.org/10.1021/acs.iecr.4c03563
Ind. Eng. Chem. Res. 2025, 64, 2816−2830